Breaking universality in random sequential adsorption on a square lattice with long-range correlated defects

Sumanta Kundu [1,*] and Dipanjan Mandal [2,†]
[1]*Department of Earth and Space Science, Osaka University, 560-0043 Osaka, Japan*
[2]*Department of Physics, University of Warwick, Coventry CV4 7AL, United Kingdom*

(Received 12 February 2021; accepted 7 April 2021; published 26 April 2021)

Jamming and percolation transitions in the standard random sequential adsorption of particles on regular lattices are characterized by a universal set of critical exponents. The universality class is preserved even in the presence of randomly distributed defective sites that are forbidden for particle deposition. However, using large-scale Monte Carlo simulations by depositing dimers on the square lattice and employing finite-size scaling, we provide evidence that the system does not exhibit such well-known universal features when the defects have spatial long-range (power-law) correlations. The critical exponents ν_j and ν associated with the jamming and percolation transitions, respectively, are found to be nonuniversal for strong spatial correlations and approach systematically their own universal values as the correlation strength is decreased. More crucially, we have found a difference in the values of the percolation correlation length exponent ν for a small but finite density of defects with strong spatial correlations. Furthermore, for a fixed defect density, it is found that the percolation threshold of the system, at which the largest cluster of absorbed dimers first establishes the global connectivity, gets reduced with increasing the strength of the spatial correlation.

DOI: 10.1103/PhysRevE.103.042134

I. INTRODUCTION

The study of adsorption of particles onto solid surfaces is a subject of great interest in different disciplines of science and technology [1–4] due to its relevance in diverse applications, including protein adsorption [5], ion implantation in semiconductors [6], and thin film deposition technologies for surface coatings and encapsulations [7]. In the simplest case of adsorption leading to monolayer formation, such as the binding of protein molecules on glass or metals [2], one considers that the process of adsorption takes place irreversibly and the particles have no mobility. Consequently, they remain at their position of adsorption forever. However, many complex dynamical phenomena, such as diffusion, desorption, and thermal expansion of particles, are often found to be associated with the process of adsorption occurring in the real-world systems [8–10]. It has been observed that such underlying mechanisms crucially affect the morphology of the growing monolayer formations. Apart from that, properties of the surface, for example, the surface roughness or the interfacial interaction play a significant role in the kinetics of adsorption [11]. However, to our knowledge, the latter aspects have not been studied in great detail using theoretical models.

The theoretical study of monolayer formation in the limit of irreversible adsorption has been carried out quite intensively over the last several decades through the stochastic models of random sequential adsorption (RSA) [1,12,13]. In the standard RSA, particles are absorbed sequentially and irreversibly at random positions onto an initially empty substrate, subject to a constraint that they only interact through excluded volume interaction. The kinetics of adsorption terminates when a jamming state is reached where no more vacant space is available to accommodate a single particle. The surface coverage p, defined as the volume fraction of the surface occupied by the adsorbed particles, attains a nontrivial value p_j at the jamming limit. The exact value of p_j is known only for one-dimensional systems in both continuum and lattice spaces [14,15].

Another important aspect which has been studied using the RSA model is the phenomenon of percolation of polyatomic species [16–19]. A group of adsorbed particles, occupying more than one lattice site, forms clusters through their neighboring connections. The percolation transition occurs when such a cluster connects two opposite boundaries of the system through a spanning path at a critical value of the surface coverage $p = p_c$, known as the percolation threshold. Therefore the global connectivity exists in the system only in the percolating phase of $p > p_c$. The system exhibits the generic scale-invariant features of a continuous phase transition right at p_c [20].

Furthermore, the role played by the shape and size of the depositing particles on the morphology of the growing structure has been studied [16,18,21–23]. Different mechanisms of adsorption have also been introduced to explain various experimental observations comprehensively [10,24–26]. It has been revealed that the jamming density p_j and the percolation threshold p_c depend nontrivially on all these factors. However, interestingly, the critical behavior of the system associated with the two transition points is found to be universal, meaning that it is characterized by a universal set of

*sumanta@spin.ess.sci.osaka-u.ac.jp
†dipanjan.mandal@warwick.ac.uk

critical exponents that is independent of all these microscopic details. In all these cases, the percolation transition belongs to the ordinary percolation universality class [17–19,22,25,26]. Similarly, the jamming transition is characterized by the universal exponent ν_j relating to the size scaling of the width Δ of the transition zone, which scales with linear size L of the substrate in a spatial dimension d as $\Delta \sim L^{-1/\nu_j}$, with $\nu_j = 2/d$. The robustness of this universal scaling law has been examined on the Euclidean and fractal lattice geometries [27,28].

Although the effect of particle properties on the kinetics of adsorption have been extensively studied in the past, a theoretical investigation on the role of surface properties has remained almost unexplored. In this context, some previous studies have considered that the surface on which the adsorption is taking place is not ideal. It contains defects or impurities at random places [28–33], indicating that the binding strength of particles at these locations is so negligible that they cannot be attached there. Except for these places the adsorption is possible if the vacant space is large enough to accommodate a particle. Even in this case, the universal behavior of the RSA model is preserved. However, in many realistic situations, a surface shows spatially correlated properties [34–36] and thus the existence of spatial correlations among the defects is a more natural consideration than the randomly distributed defects. Surprisingly, this aspect has not been considered yet.

In this paper we provide a detailed study on the jamming and percolation properties of the RSA model in the presence of spatially long-range (power-law) correlated defects. Our main interest is to see whether this spatial correlation affects the critical behavior of the transitions. We found that in the regime of nonvanishing spatial correlation among the defects, the model does not exhibit the well-known universal features of the RSA. The critical exponents associated with the jamming and percolation transitions are observed to vary systematically with the strength of the spatial correlation.

II. MODEL

We consider the RSA model on a two-dimensional square lattice of size $L \times L$ with periodic boundary conditions along both directions. Particles in the form of k-mers, occupying k consecutive lattice sites along horizontal or vertical direction, are adsorbed one by one following the rules of the standard RSA onto the lattice consisting of defects which are spatially correlated. Specifically, the defective sites are located in such a manner that the correlation function between a pair of defected sites decays in the form of a power law of the spacial distance between them. By imposing this prerequisite, sites of an empty lattice are occupied with probability q and they are kept vacant with probability $1 - q$ (the detailed method for generating such a correlated landscape is described later). The initial configuration of these sets of occupied sites acts as defects and the adsorption of particles on these locations is completely forbidden. The remaining $1 - q$ fraction of sites acts as the site for possible adsorption. By selecting an orientation, either horizontal or vertical with equal probability, one end of the particle is placed at a randomly selected position and absorbed irreversibly, provided that there exists at least k consecutive vacant sites along the chosen direction from the selected site. The surface coverage after adsorbing n particles is thus given by $p = nk/L^2$. The adsorption process continues in this way until a jamming state is reached. The corresponding surface coverage $p = p_j$ is referred to as the jamming density.

During the process of adsorption, the depositing particles interact among the previously adsorbed particles as well as with the defects via excluded volume interaction. Consequently, they experience a "screening effect" and try to align parallel to each other and form domains whose typical sizes are of the order of the size of the particle. In addition, due to this interaction, a vacant region that is smaller than the size of the particle cannot be occupied. As a result, the jamming density p_j cannot attain the close packing density, i.e., $p_j < 1 - q$.

As an important step, besides the defect density parameter q, the strength of the correlation among the defects is also a tunable parameter in our model and it is characterized by an exponent γ associated with the power-law decay of the correlation function [see Eq. (1)]. For any arbitrary value of $0 < q < 1$, the strength of the correlation decreases with increasing the value of γ, and in the limit of $\gamma \to \infty$ the scenario of uncorrelated defects is obtained. Therefore, by varying the parameters q and γ, the model is capable of capturing the behavior of a wide range of systems: from a system with correlated defects, uncorrelated defects to a pure (defect-free) system. In this paper we report our simulation results for dimers ($k = 2$).

A. Generating long-range correlated defects

To obtain a substrate that possesses defects with spatial long-range correlations, we utilize the idea of viewing the substrate as a landscape of random heights $\{h(\mathbf{x})\}$ with desired height-height correlation [37], where $h(\mathbf{x})$ represents the height associated with the lattice site positioned at $\mathbf{x}$. Accordingly, we follow the scheme described in Ref. [38], which is based on the Fourier filtering method [38–40]. The Wiener-Khintchine theorem is the basis of this method, which relates the autocorrelation function of a stationary time series to the Fourier transform of its power spectrum. The power spectral density in this case has a power-law form, and it is calculated using the two-point correlation function $c(\mathbf{r}) = (1 + |\mathbf{r}|^2)^{-\gamma/2}$, imposing periodic boundary conditions in two dimensions. Therefore $c(\mathbf{r})$ decays at large distance $|\mathbf{r}|$ as

$$c(\mathbf{r}) = \langle h(\mathbf{x})h(\mathbf{r}+\mathbf{x})\rangle \sim |\mathbf{r}|^{-\gamma}, \tag{1}$$

where γ denotes the strength of the correlation. The steps (i)–(iii) in Ref. [38] are then executed to generate the correlated random numbers $\{h(\mathbf{x})\}$.

In our simulation we used Gaussian distributed uncorrelated random numbers with zero mean and unit variance to generate power-law correlated Gaussian distributed random numbers. To verify whether the obtained random numbers posses the desired correlations or not, the configuration averaged value of $c(\mathbf{r})$ is plotted with $|\mathbf{r}|$ on a double logarithmic scale in Fig. 1 for three different values of γ. Clearly, the measured slopes of the best fitted straight lines are consistent with the desired values of γ.

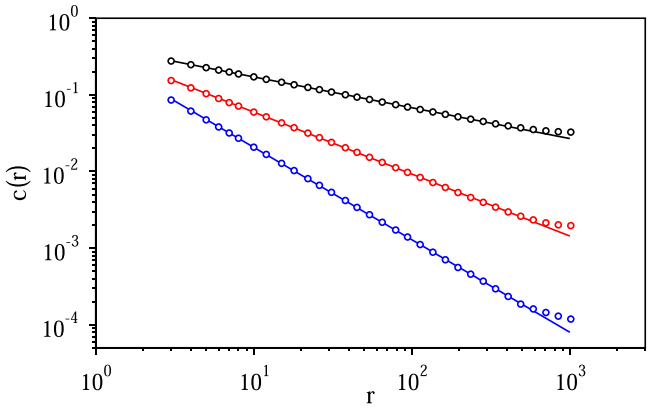

FIG. 1. Log-log plot of the height-height correlation function $c(\mathbf{r})$ against the spatial distance $|\mathbf{r}|$ on a two-dimensional surface with $L = 2^{11}$ using $\gamma = 0.4$ (black), 0.8 (red), and 1.2 (blue) (open circles). By averaging over 10^4 independent configurations, the slope of the fitted straight lines have been estimated as 0.408(5), 0.804(5), and 1.206(5), respectively (arranged from top to bottom).

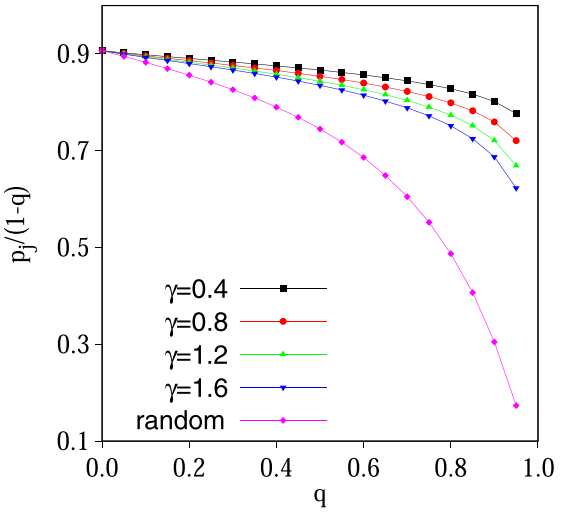

FIG. 3. The variation of filling fraction $p_j/(1-q)$ against the defect density q for $\gamma = 0.4$, 0.8, 1.2, 1.6 and uncorrelated defects using $L = 1024$.

Finally, by following the idea of ranked surface [41], the sites are occupied one by one according to the ascending order of their height values until the density of occupied sites representing the defects reaches a prefixed value q.

III. RESULTS

A. Impact on the jamming coverage

In Fig. 2 we have shown typical jamming configurations for a given defect density q for both correlated and uncorrelated defects. We first observe that the defects form clusters via nearest-neighbor connections, which become more and more compact for stronger correlations (small γ). An idea of the compactness of the clusters may quantitatively be realized from the fact that in the subcritical regime of defect density, i.e., for $q < q_c$, where the global connectivity through the clusters of defects is absent, the average size of the largest cluster of defects scales with L as $\langle s_{\max}^{\text{def}}(L)\rangle \sim (\ln(L))^{\alpha}$ (not shown). It is found that the exponent $\alpha > 1$ for $0 < \gamma < d$,

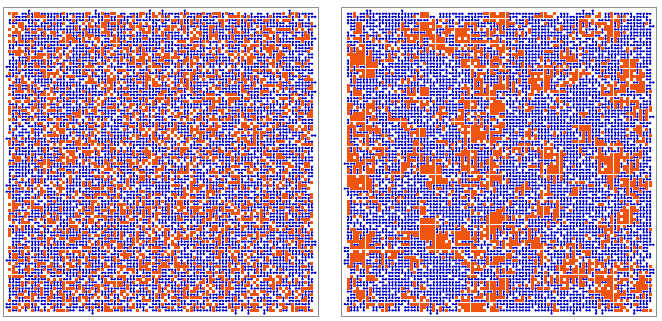

(a) (b)

FIG. 2. Typical jamming configurations of dimers on a 96×96 lattice with periodic boundary conditions using defect density $q = 0.3$ for (a) uncorrelated and (b) correlated defects with $\gamma = 0.4$. The sites with defects and the absorbed dimers have been painted in orange squares and blue circles, respectively.

which monotonically decreases with increasing the value of γ. This finally approaches $\alpha = 1$, corresponding to the value for uncorrelated defects.

Naturally, the particles experience the strongest screening effect in the case of homogeneously distributed uncorrelated defects during the deposition, and it recedes as the strength of the correlation is increased. Thus we expect to observe densely packed jamming states for stronger correlations. To demonstrate this, the filling fraction $p_j/(1-q)$ at the jamming state is plotted against q in Fig. 3 for four different values of γ and for uncorrelated defects. Clearly, for any given value of $0 < q < 1$, the filling fraction increases as the value of γ decreases.

B. Universality class of the jamming transition

To investigate whether the universality class of the jamming transition is affected by the introduction of spatial correlations among the defects, we perform the scaling analysis of the width $\Delta(L)$ of the transition zone. Precisely, we calculate the standard deviation of the jamming densities $\Delta(L) = \sqrt{\langle p_j^2\rangle - \langle p_j\rangle^2}$ for several values of L, which generally scales as $\Delta(L) \sim L^{-1/\nu_j}$. Therefore we plot $\Delta(L)$ versus L on a log-log scale. We simulate up to $L = 4096$, and the averaging was done on (at least) 5×10^6, 9.5×10^5, 1.5×10^5, 3×10^4, and 6×10^3 independent configurations for $L = 256$, 512, 1024, 2048, and 4096, respectively. It is observed that the curves for small γ have a certain amount of curvatures, and they seem to approach a constant value in the limit $L \to \infty$. We thus consider a modified functional form

$$\Delta(L) = AL^{-1/\nu_j} + B \tag{2}$$

to fit our data. Indeed, a plot of $\Delta(L) - B$ against L on a double logarithmic scale exhibits a straight line, as shown in Fig. 4. It is found that $B \approx 0$ for $\gamma \gtrsim 1.0$, but its value increases monotonically as γ is decreased. To give an idea, the least-squares fit of our data using Eq. (2) yields the values of $(1/\nu_j, B) \approx (0.97, 4.63 \times 10^{-6})$, $(0.95, 2.66 \times 10^{-5})$, and

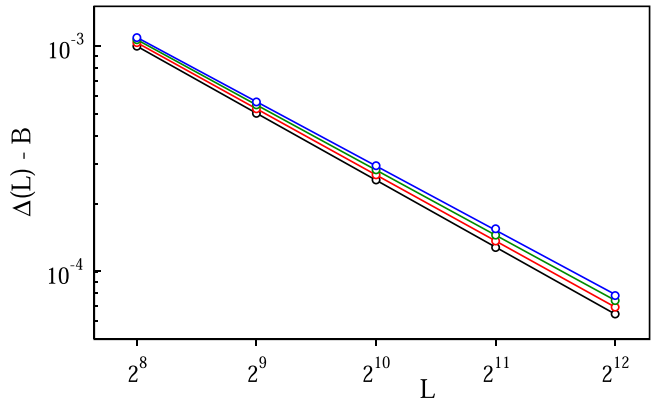

FIG. 4. Plot of $\Delta(L) - B$ against L on a log-log scale for $\gamma = 0.8$. The slope of the best-fitted straight lines have been estimated as $1/\nu_j = 0.987(2), 0.974(4), 0.962(5)$, and $0.944(5)$ for $q = 0.1$, 0.2, 0.3, and 0.4, respectively (arranged from bottom to top). The corresponding values of B are smaller than $B = 9.771\,82 \times 10^{-6}$ for $q = 0.4$.

$(0.92, 9.31 \times 10^{-5})$ for $\gamma = 0.8$, 0.6, and 0.4, respectively, using $q = 0.2$. As opposed to the case of uncorrelated defects, for which one obtains the universal value of $\nu_j = 1$ in two dimensions at any arbitrary value of $0 < q < 1$, it is evident from Fig. 4 that the exponent ν_j varies systematically with q for a fixed γ.

Similar plots are made, but now we keep q fixed and vary γ. To show the effect of the spatial correlation more explicitly, we focus on the range of $q < q_c$, where there exists no giant cluster of defects. It is found that the deviation of ν_j from its universal value $\nu_j = 1$ becomes more and more prominent as $\gamma \to 0$ (strong correlations). In Fig. 5 we have displayed such a plot for three different values of q. Although the nonuniversal behavior is not so obvious from this figure for $q = 0.05$ as the exponent value is close to $\nu_j = 1$, the curves have apparent curvatures on the $\Delta(L)$ vs L plots for small γ. Precisely, the best fit using Eq. (2) yields a value of $B > 0$ (e.g., $B \approx 2.1981 \times 10^{-5}$ for $\gamma = 0.4$ and $q = 0.05$). This suggests that a small but finite amount of defects (i.e., $q > 0$) is sufficient to change the universal behavior of the jamming transition if and only if the defects have strong spatial correlations.

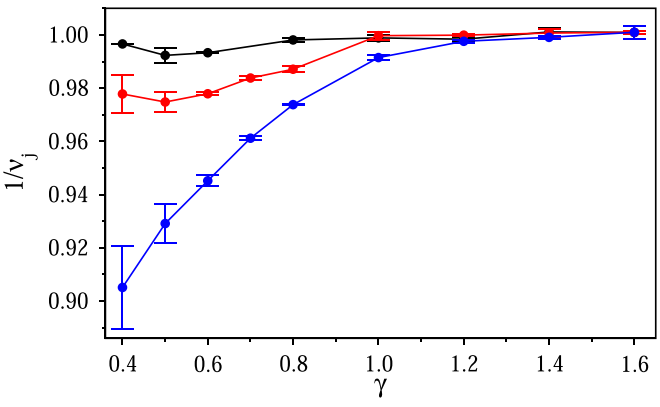

FIG. 5. Variation of the critical exponent $1/\nu_j$ associated with the jamming transition as a function of the correlation strength γ for $q = 0.05$ (black), 0.10 (red), and 0.20 (blue) (arranged from top to bottom).

What could be the reason behind the origin of this nonuniversal behavior? One may notice from Fig. 2 that for strong spatial correlations, the void space becomes fragmented into several isolated clusters and forms islands surrounded by defects. This happens even for a small value of q (e.g., $q = 0.1$), while they are less likely to be formed in the case of uncorrelated defects at such small densities. The shapes and sizes of these islands vary for different configurations. The size distribution appears to be broad even for $q = 0.1$, and the tail of the distribution is observed to shift to the origin with increasing γ (weak correlations). Besides that, the total number of islands also varies for different configurations. Since the particle adsorption is occurring on these islands, one may think that the fluctuation of the jamming densities for a given system size L is a collective contribution of the fluctuations arising from all those islands. Thus the variability of the island sizes could be the source of breaking the universality class of the jamming transition.

Arguably, such a scenario also arises at the percolation point of void spaces in the presence of uncorrelated defects, where the size distribution of those islands follows a scale-free distribution. However, using extensive numerical simulations by setting $1 - q = 0.592\,746\,050$ (percolation threshold of the square lattice), we have obtained the universal value of $\nu_j = 1$ (not shown). This suggests that the departure from the universal behavior for long-range spatially correlated defects is probably not due to the above-mentioned fluctuations and could be related to some more complex details, such as spatial correlations between the sizes of the islands or the nontrivial interactions of particles in the close proximity to the complex inner and outer wall of the compact clusters of defects. Furthermore, we have noticed that the distribution of p_j deviates from a Gaussian distribution for strongly correlated defects for large system sizes.

C. Percolation transition of the jamming states

We now identify the clusters of absorbed dimers in the jamming state, where a cluster consists of a set of sites interconnected through their neighboring sites occupied by the dimers. For $q = 0$, the density of occupied sites is so high ($p_j \approx 0.9068$) that there always exists global connectivity through a cluster spanning the entire system. On the other hand, at $q = q_c$, when a giant cluster of defects first appears in the system, the largest cluster of dimers becomes minuscule and it fails to establish such global connectivity. Consequently, in between $q = 0$ and q_c, one finds a threshold value of $q = q_{cj}$ such that the system of dimers exhibits the global connectivity and thus remains in the percolating phase only when $q < q_{cj}$. In the range of $q_{cj} < q < q_c$, neither the largest cluster of dimers nor defects percolates. The schematic phase diagram in q plane is shown in Fig. 6.

The most important question here is whether the critical behavior of such a percolation transition occurring at $q = q_{cj}$ belongs to the ordinary percolation universality class when the defects have spatial long-range correlations. To investigate this, we calculate the spanning probability $\Pi(q, L)$ that there

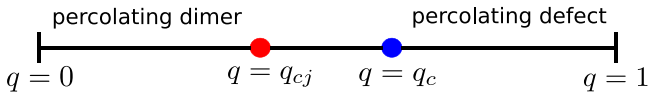

FIG. 6. Schematic phase diagram in one-dimensional q plane. Red and blue dots represent the critical point of percolation through the dimers and defects, respectively. In the region between the two dots, the system percolates neither through dimers nor through defects.

exists a spanning cluster of adsorbed dimers in the system by varying the value of q for three different system sizes L. Then, by performing the finite-size scaling analysis of $\Pi(q, L)$ and estimating the scaling exponents we determine the universality class of the percolation transition. Once a jamming configuration is reached in our simulation, we check the top to bottom connectivity through the neighboring sites occupied by the dimers using the Burning algorithm [20] imposing periodic (open) boundary conditions along the horizontal (vertical) direction. It may be noted that the dimers adsorbed in the isolated small islands of void space do not help in achieving the global connectivity. Only the largest island of void space holds a special importance for this purpose, whose size in its percolating phase scales as $\langle s^{\rm vac}_{\rm max}(L)\rangle = (a + b/\ln(L))L^2$ (not shown). In the context of percolation of adsorbed dimers, this may signify an effective change in the dimensionality of

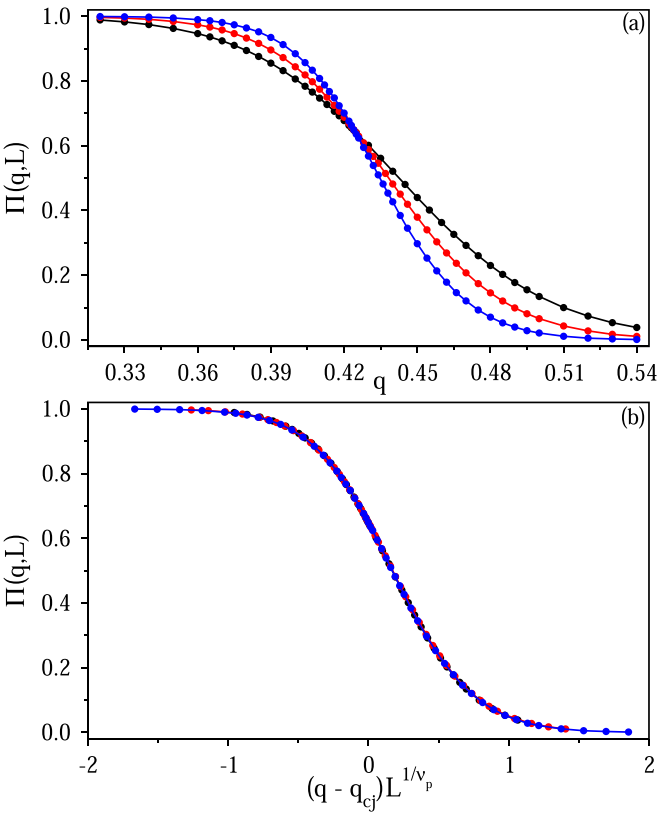

FIG. 7. For $\gamma = 0.8$, (a) variation of the spanning probability $\Pi(q, L)$ of the jamming configuration with defect density q for system sizes $L = 256$ (black), 512 (red), and 1024 (blue) (from left to right along $\Pi = 0.8$); (b) finite-size scaling plot of the same data using $q_{cj} = 0.4241(2)$ and $1/\nu_p = 0.400(5)$.

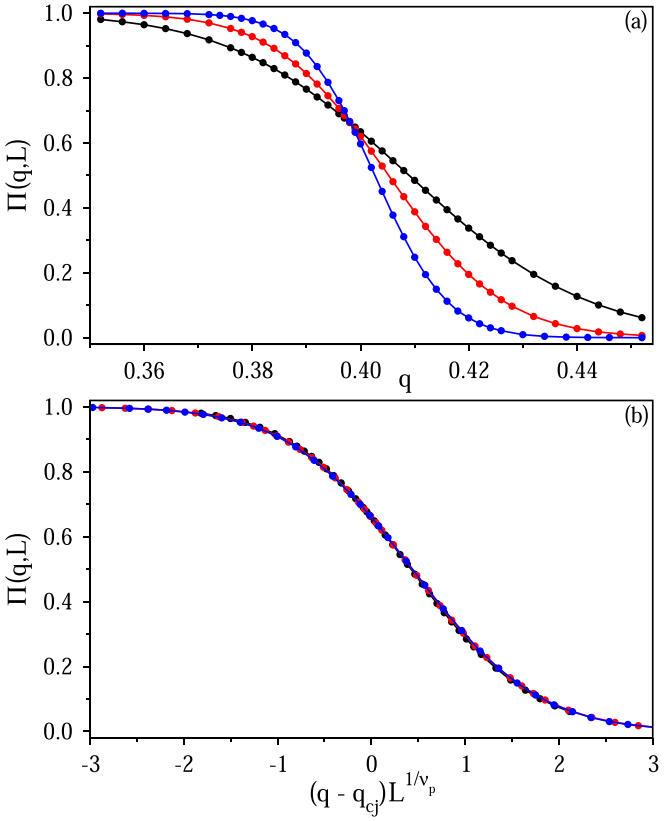

FIG. 8. For $\gamma = 1.5$, (a) variation of the spanning probability $\Pi(q, L)$ of the jamming configuration with defect density q for system sizes $L = 256$ (black), 512 (red), and 1024 (blue) (from left to right along $\Pi = 0.8$); (b) finite-size scaling plot of the same data using $q_{cj} = 0.3982(2)$ and $1/\nu_p = 0.662(5)$.

the problem. In general, $b > 0$ for strong correlations, but its value decreases monotonically and approaches to zero (the value in the case of uncorrelated defects) as γ increases.

In Fig. 7(a), the variation of the spanning probability $\Pi(q, L)$ against q has been shown for $\gamma = 0.8$. By appropriately scaling the horizontal axis, when the same sets of data are replotted against $(q - q_{cj})L^{1/\nu_p}$ we observe a nice data collapse [Fig. 7(b)], implying the finite-size scaling form

$$\Pi(q, L) \sim \mathcal{F}[(q - q_{cj})L^{1/\nu_p}], \tag{3}$$

where ν_p is recognized as the correlation length exponent of the percolation transition. The analysis yields $q_{cj} = 0.4241(2)$ and $1/\nu_p = 0.400(5)$ for $\gamma = 0.8$. We have also shown similar plots for $\gamma = 1.5$ in Figs. 8(a) and 8(b). In this case we obtained $q_{cj} = 0.3982(2)$ and $1/\nu_p = 0.662(5)$. It is evident that these exponent values are distinctly different from the value of $1/\nu_p = 0.75$ for uncorrelated defects, for which such a transition belongs to the ordinary percolation universality class in two dimensions.

Repeating these analyses for many different values of γ, we see that the critical exponent $1/\nu_p$ increases with increasing γ and approaches to $1/\nu_p = 3/4$, as shown in Fig. 9(a). This dependency is approximately described by a relation $\nu_p = 2/\gamma$ in the range of $\gamma = 0.6$–1.0. The percolation threshold $q_{cj}(\gamma)$ decreases with increasing γ and approaches 0.3180(5), the value for uncorrelated defects, as shown in

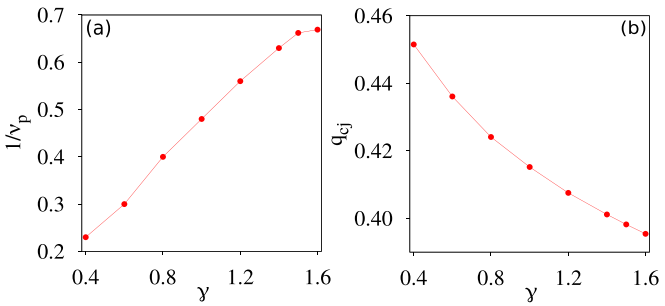

FIG. 9. Variation of (a) the critical exponent ν_p associated with the percolation transition of the jamming states and (b) the percolation threshold q_{cj} as a function of γ.

Fig. 9(b). Note that our results for uncorrelated defects are in good agreement with the previous numerical data in Ref. [32]. The data used for all these plots are based on averages over (at least) 10^6, 5×10^5, and 7×10^4 samples for $L = 256$, 512, and 1024, respectively. Therefore we believe that the above estimates are reasonably accurate.

D. Percolation transition before jamming

We have seen that for a given value of γ, the defect density $q = q_{cj}(\gamma)$ separates between the percolating and nonpercolating jamming states. Specifically, all the jamming configurations for $q < q_{cj}(\gamma)$ with density $p_j(\gamma, q)$ percolate in the limit of asymptotically large system sizes. This suggests that for all values of $q < q_{cj}(\gamma)$ there should be a critical value of $p = p_c(\gamma, q)$ such that the system exhibits global connectivity for $p_c(\gamma, q) \leqslant p \leqslant p_j(\gamma, q)$.

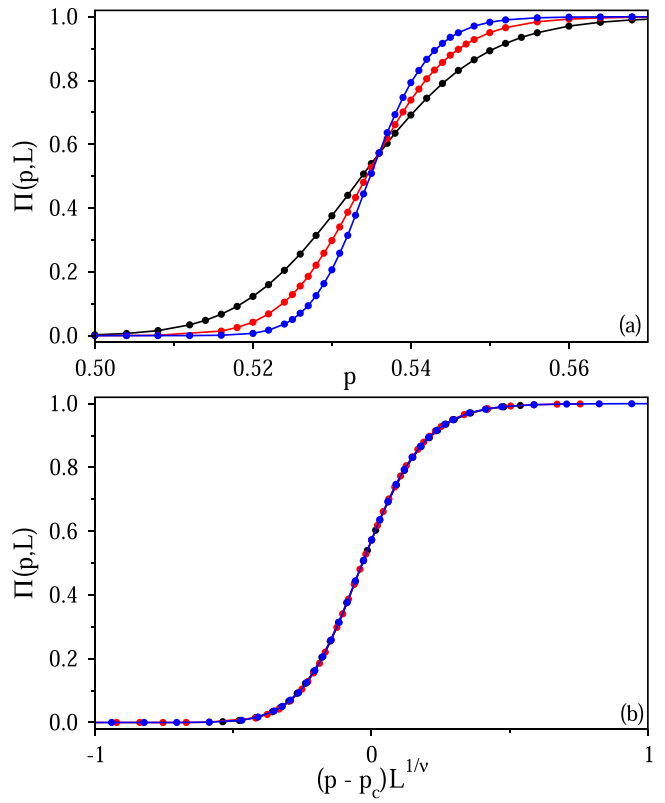

FIG. 10. For $\gamma = 0.8$, $q = 0.1$, (a) the spanning probability $\Pi(p, L)$ has been plotted against the surface coverage p for system sizes $L = 256$ (black), 512 (red), and 1024 (blue) (from left to right along $\Pi = 0.2$). (b) Finite-size scaling of the same data as in (a) using $p_c = 0.535\,95(3)$ and $1/\nu = 0.488(5)$.

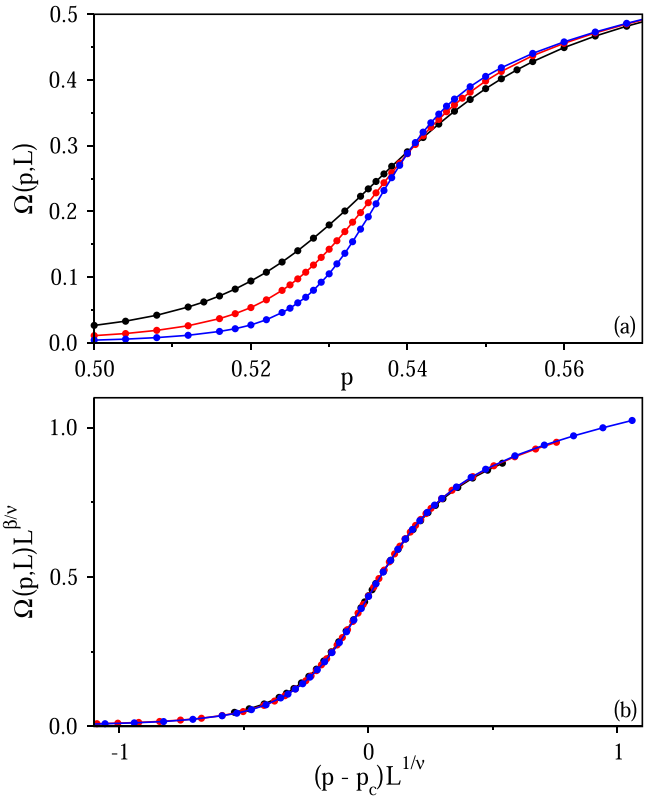

FIG. 11. For $\gamma = 0.8$, $q = 0.1$, (a) variation of the order parameter $\Omega(p, L)$ against the surface coverage p for system sizes $L = 256$ (black), 512 (red), and 1024 (blue) (from left to right along $\Pi = 0.2$). (b) Finite-size scaling of the same data as in (a) using $p_c = 0.535\,95(3)$, $1/\nu = 0.488(5)$, and $\beta/\nu = 0.104(1)$.

In Fig. 10(a) we have plotted the spanning probability $\Pi(p, L)$ against the surface coverage p for three different system sizes using $\gamma = 0.8$ and $q = 0.1$. These curves cross each other approximately at a single point $[p_c(\gamma, q), \Pi(p_c)]$. From visual inspection, we estimate that $p_c(0.8, 0.1) = 0.535\,95(3)$ and $\Pi(p_c) \approx 0.57$, which is quite lower than the value 0.636454001 of the crossing probability on a cylindrical geometry obtained using Cardy's formula [42,43] for defect-free systems. It is to be noted that the crossing probability $\Pi(p_c) \approx 0.64$ has been obtained even for the system with uncorrelated defects. Now a finite-size scaling of the same data is performed. A plot of $\Pi(p, L)$ against the scaled variable $(p - p_c(\gamma, q))L^{1/\nu}$ exhibits the data collapse for all three system sizes [Fig. 10(b)], implying the scaling form

$$\Pi(p, L) \sim \mathcal{F}[(p - p_c(\gamma, q))L^{1/\nu}]. \tag{4}$$

In percolation problems, the average size of the largest cluster per site is considered as the order parameter $\Omega(p, L) = \langle s_{\max}(p, L)\rangle/L^2$, where $s_{\max}$ represents the size of the largest cluster of absorbed dimers. In Fig. 11(a) we have shown the variation of $\Omega(p, L)$ against p for the same three system sizes.

TABLE I. Our numerical estimates of the percolation threshold $p_c(\gamma, q)$ for different values of the defect density q and the correlation strength γ. The numbers in the parentheses represent the error bars in the last digit.

γ	q	$p_c(\gamma, q)$	$1/\nu$	β/ν
0.6	0.01	0.55965(3)	0.71(1)	0.105(1)
	0.01	0.56022(3)	0.718(5)	0.104(1)
0.8	0.05	0.54986(3)	0.587(5)	0.104(1)
	0.10	0.53595(3)	0.488(6)	0.104(1)
	0.01	0.56083(2)	0.735(5)	0.104(1)
1.2	0.05	0.55362(2)	0.671(6)	0.105(1)
	0.10	0.54329(3)	0.621(5)	0.104(1)

Again, by appropriately scaling the abscissa and ordinate, and replotting the data we observe data collapse of $\Omega(p, L)$, as shown in Fig. 11(b), indicating the scaling form

$$\Omega(p, L)L^{\beta/\nu} \sim \mathcal{G}[(p - p_c(\gamma, q))L^{1/\nu}]. \tag{5}$$

The finite-size scaling analysis yields $p_c(0.8, 0.1) = 0.535\,95(3)$, $1/\nu = 0.488(5)$, and $\beta/\nu = 0.104(1)$. These values are compared with the known critical exponents for ordinary percolation in two dimensions, which are $1/\nu = 3/4$ and $\beta = 5/36$.

The above set of calculations has been repeated for different (γ, q) pairs. Interestingly, we found that the critical exponent $1/\nu$ depends systematically with q and γ, whereas β/ν always appears to be same as the value of the ordinary percolation in two dimensions, i.e., $\beta/\nu = 5/48$. The estimated values for different (γ, q) pairs are listed in Table I. For strong correlations ($\gamma \leqslant 0.6$) and high q, it is observed that the crossing points of the curves for $\Pi(p, L)$ vary over a much wider range. In these cases, the two-parameter scaling plot does not exhibit an excellent data collapse as seen for $\gamma \geqslant 0.8$. Probably, logarithmic corrections are responsible for this. Further investigations using higher system sizes are thus needed for a precise understanding of this problem.

IV. CONCLUSIONS

We have investigated the percolation and jamming properties of the random sequential adsorption of dimers on square lattices in the presence of defects with spatial long-range correlations. Accordingly, a fraction q of the lattice sites are declared as defects, where the deposition of dimers is completely forbidden. The dimer adsorption takes place randomly at the available vacant space. The correlation strength among the defective sites is varied, and its impact on the jamming and percolation transitions has been studied using extensive numerical simulations.

It has been observed that the jamming coverage for any arbitrary value of $0 < q < 1$ is increased with increasing correlation strength. More importantly, for strong correlations the jamming transition is found to be nonuniversal, even when q is much smaller than its threshold value q_c such that the connected clusters of defects are all minuscule. A continuously tunable value of ν_j characterizes the jamming transition, which approaches its universal value $\nu_j = 1$ in two dimensions with decreasing correlation strength.

The percolation transition of the absorbed dimers takes place at a critical density of occupied sites p_c only when the defect density is smaller than a critical value $q = q_{cj}$. The percolation threshold p_c has been found to be dependent on the defect density as well as the strength of the spatial correlations. For a given defect density, p_c decreases as the correlation strength is increased. Moreover, the finite-size scaling analysis reveals that the transition does not belong to the ordinary percolation universality class. The correlation length exponent ν changes systematically with the strength of the spatial correlation and approaches its universal value $4/3$ in two dimensions when the defects become weakly correlated. Remarkably, the ratio of the exponents β/ν associated with the order parameter scaling appears to remain the same as the ordinary percolation.

Finally, by tuning the defect density q, a percolation transition is observed at $q = q_{cj}$ which separates the percolating jamming states from the nonpercolating ones. Again, the percolation transition is characterized by a nonuniversal value of the correlation length exponent, which is found to be dependent on the strength of the spatial correlation among the defects.

In the future, apart from the obvious generalization of this model by considering different shapes and sizes of the particles on different lattice geometries or in higher dimensions, one may find it interesting to study precursor-mediated adsorption in such a correlated disordered environment. We are hopeful that the results presented here will provide a framework for understanding various observations in different experimental conditions more coherently, since by tuning the parameters (q and γ) of the model a system resembling the real one may be devised.

ACKNOWLEDGMENTS

We sincerely thank Nuno A. M. Araújo for a critical review of the manuscript and A. J. Ramirez-Pastor for suggesting to us interesting papers on the subject. S.K. acknowledges support from the Japan Society for the Promotion of Science (JSPS) Grants-in-Aid for Scientific Research (KAKENHI) Grants No. JP16H06478 and No. 19H01811. Additional support from the MEXT under "Exploratory Challenge on Post-K computer" (Frontiers of Basic Science: Challenging the Limits) and the "Earthquake and Volcano Hazards Observation and Research Program" is also gratefully acknowledged. D.M. acknowledges support from a EPSRC Programme Grant (Grant No. EP/R018820/1) which funds the Crystallization in the Real World consortium. In addition, D.M. gratefully acknowledges use of the computational facilities provided by the University of Warwick Centre for Scientific Computing.

[1] J. W. Evans, Rev. Mod. Phys. **65**, 1281 (1993).

[2] J. Feder, J. Theor. Biol. **87**, 237 (1980).

[3] S. Torquato and F. H. Stillinger, Rev. Mod. Phys. **82**, 2633 (2010).
[4] E. Kumacheva, R. Golding, M. Allard, and E. Sargent, Adv. Mater. **14**, 221 (2002).
[5] V. Hlady and J. Buijs, Curr. Opin. Biotechnol. **7**, 72 (1996).
[6] E. Roman and N. Majlis, Solid State Commun. **47**, 259 (1983).
[7] D. Yu, Y.-Q. Yang, Z. Chen, Y. Tao, and Y.-F. Liu, Opt. Commun. **362**, 43 (2016).
[8] V. Privman, Trends Stat. Phys. **1**, 89 (1994).
[9] J. J. Ramsden, J. Phys. Chem. **96**, 3388 (1992).
[10] D. Joshi, D. Bargteil, A. Caciagli, J. Burelbach, Z. Xing, A. S. Nunes, D. E. Pinto, N. A. Araújo, J. Brujic, and E. Eiser, Sci. Adv. **2**, e1600881 (2016).
[11] S. Napolitano, Soft Matter **16**, 5348 (2020).
[12] V. Privman, J. Adhes. **74**, 421 (2000).
[13] A. Cadilhe, N. A. M. Araújo, and V. Privman, J. Phys.: Condens. Matter **19**, 065124 (2007).
[14] P. J. Flory, J. Am. Chem. Soc. **61**, 1518 (1939).
[15] A. Rényi, Publ. Math. Inst. Hung. Acad. Sci. **3**, 109 (1958).
[16] G. Kondrat and A. Pekalski, Phys. Rev. E **63**, 051108 (2001).
[17] V. Cornette, A. J. Ramirez-Pastor, and F. Nieto, Eur. Phys. J. B **36**, 391 (2003).
[18] Y. Y. Tarasevich, N. I. Lebovka, and V. V. Laptev, Phys. Rev. E **86**, 061116 (2012).
[19] M. Gimenez and A. Ramirez-Pastor, Physica A **421**, 261 (2015).
[20] D. Stauffer and A. Aharony, *Introduction To Percolation Theory* (Taylor & Francis, London, 2018).
[21] J. Becklehimer and R. B. Pandey, Physica A **187**, 71 (1992).
[22] N. I. Lebovka, N. N. Karmazina, Y. Y. Tarasevich, and V. V. Laptev, Phys. Rev. E **84**, 061603 (2011).
[23] M. Cieśla, G. Pajaąk, and R. M. Ziff, J. Chem. Phys. **145**, 044708 (2016).
[24] X.-C. Guo, J. Bradley, A. Hopkinson, and D. King, Surf. Sci. **310**, 163 (1994).
[25] S. Kundu, N. A. M. Araújo, and S. S. Manna, Phys. Rev. E **98**, 062118 (2018).
[26] A. P. Furlan, D. C. dos Santos, R. M. Ziff, and R. Dickman, Phys. Rev. Research **2**, 043027 (2020).
[27] P. M. Pasinetti, L. S. Ramirez, P. M. Centres, A. J. Ramirez-Pastor, and G. A. Cwilich, Phys. Rev. E **100**, 052114 (2019).
[28] L. S. Ramirez, P. M. Centres, and A. J. Ramirez-Pastor, J. Stat. Mech.: Theory Exp. (2019) 033207.
[29] V. Cornette, A. Ramirez-Pastor, and F. Nieto, Phys. Lett. A **353**, 452 (2006).
[30] G. Kondrat, J. Chem. Phys. **124**, 054713 (2006).
[31] P. M. Centres and A. J. Ramirez-Pastor, J. Stat. Mech.: Theory Exp. (2015) P10011.
[32] Y. Y. Tarasevich, V. V. Laptev, N. V. Vygornitskii, and N. I. Lebovka, Phys. Rev. E **91**, 012109 (2015).
[33] G. Palacios and M. A. F. Gomes, J. Phys. A: Math. Theor. **53**, 375003 (2020).
[34] E. Medina, T. Hwa, M. Kardar, and Y.-C. Zhang, Phys. Rev. A **39**, 3053 (1989).
[35] T. A. Hewett and R. A. Behrens, SPE Form. Eval. **5**, 217 (1990).
[36] K. B. Lauritsen, M. Sahimi, and H. J. Herrmann, Phys. Rev. E **48**, 1272 (1993).
[37] K. J. Schrenk, N. Posé, J. J. Kranz, L. V. M. van Kessenich, N. A. M. Araújo, and H. J. Herrmann, Phys. Rev. E **88**, 052102 (2013).
[38] H. A. Makse, S. Havlin, M. Schwartz, and H. E. Stanley, Phys. Rev. E **53**, 5445 (1996).
[39] S. Prakash, S. Havlin, M. Schwartz, and H. E. Stanley, Phys. Rev. A **46**, R1724 (1992).
[40] J. Zierenberg, N. Fricke, M. Marenz, F. P. Spitzner, V. Blavatska, and W. Janke, Phys. Rev. E **96**, 062125 (2017).
[41] K. J. Schrenk, N. A. M. Araújo, J. S. Andrade, Jr., and H. J. Herrmann, Sci. Rep. **2**, 348 (2012).
[42] J. Cardy, J. Stat. Phys. **125**, 1 (2006).
[43] R. M. Ziff, Phys. Rev. E **83**, 020107(R) (2011).